NEOPLASIA
www.neoplasia.com

Volume 13 Number 1 January 2011 pp. 31–39 31

Augmented Osteolysis in SPARC-Deficient Mice with Bone-Residing Prostate Cancer[1,2,3]

N. Patrick McCabe*[,4,5], Bethany A. Kerr*[,4], Maria Madajka*[,6], Amit Vasanji[†] and Tatiana V. Byzova*[,‡]

*Department of Molecular Cardiology, Joseph J. Jacobs Center for Thrombosis and Vascular Biology, Lerner Research Institute, Cleveland Clinic Foundation, Cleveland, OH, USA; [†]Department of Biomedical Engineering, Lerner Research Institute, Cleveland Clinic Foundation, Cleveland, OH, USA; [‡]Taussig Cancer Center, Cleveland Clinic Foundation, Cleveland, OH, USA

Abstract

Prostate cancer preferentially metastasizes to bone, which is rich in structural and matricellular proteins capable of altering prostate cancer progression. This study explores the role of the bone stromal matricellular protein SPARC (osteonectin/BM-40) in the progression of bone metastatic prostate cancer. Quantification of bone destruction analyzed by micro–computed tomography showed augmented osteoclastic resorption, characterized by decreases in several morphometric bone parameters in SPARC knock out (KO) tibiae harboring RM1 murine prostate cancer cells compared with wild type (WT) animals. Tumor progression stimulated osteoclast formation, which was augmented in SPARC KO mice. *In vitro* differentiation of SPARC KO osteoclasts indicated accelerated progenitor expansion and formation of tartrate-resistant acid phosphatase–positive osteoclast-like cells with increased resorptive capacity, a mechanism resulting in enhanced tumor-induced bone loss *in vivo*. Whereas altered bone structure due to SPARC KO played a role in increased osteolysis, the enhanced osteolysis was primarily the result of increased resorption by SPARC KO osteoclasts. Our findings indicate that bone stromal SPARC suppresses tumor-induced bone lesion expansion by limiting osteoclast maturation and function.

Neoplasia (2011) 13, 31–39

Abbreviations: BMMΦ, bone marrow macrophage; BSA, bone surface area; BV/TV, bone volume–to–total volume ratio; M-CSF, macrophage colony-stimulating factor; microCT, micro–computed tomography; MNC, multinucleated cell; RANKL, receptor activator of NF-κB ligand; SPARC, secreted protein acidic and rich in cysteine; Tb.Th, trabecular thickness; Tb.N, trabecular number; Tb.Sp, trabecular spacing; TRAMP, transgenic adenocarcinoma of the mouse prostate; TRAP, tartrate-resistant acid phosphatase

Address all correspondence to: Tatiana V. Byzova, PhD, Department of Molecular Cardiology, The Cleveland Clinic Lerner Research Institute, 9500 Euclid Ave NB-50, Cleveland, OH 44195. E-mail: byzovat@ccf.org

[1]This work was supported by a National Institutes of Health/National Cancer Institute grant CA126847 to T.V. Byzova. N.P. McCabe was supported by a Ruth L. Kirschstein Research Service Award Individual Fellowship (5F32 CA1172462). B.A. Kerr was supported by an institutional training grant (T32 HL007914) from the National Institutes of Health/National Heart, Lung, Blood Institute. Cleveland Clinic Biomedical Imaging and Analysis Core Center was funded in part by the National Institute of Arthritis and Musculoskeletal and Skin Diseases Core Center Grant 1P30 AR050953.

[2]The authors declare no competing financial interests.

[3]This article refers to supplementary materials, which are designated by Figures W1 to W5 and are available online at www.neoplasia.com.

[4]These authors contributed equally to this work.

[5]Present address: Department of Biomedical Engineering, Lerner Research Institute, Cleveland Clinic Foundation, Cleveland, OH 44195.

[6]Present address: Department of Plastic Surgery, Cleveland Clinic Foundation, Cleveland, OH 41195.

Received 16 July 2010; Revised 27 September 2010; Accepted 28 September 2010

DOI 10.1593/neo.10998

Introduction

Bone is a metastatic "hot spot" for several cancers including prostate [1]. Prostate cancer has the highest incidence of all cancers in Western males and accounts for 25% of reported cancers [2]. As bone metastasis affects greater than 80% of patients with advanced prostate cancer and determines patient morbidity and disease-related mortality, this phase of prostate cancer deserves considerable attention. Previous studies using prostate cancer patient tissue samples reported that SPARC (secreted protein acidic and rich in cysteine; osteonectin; BM-40) expression at metastatic sites is higher compared with that in primary sites [3–5]. SPARC is a highly expressed matricellular protein in bone, where its expression levels trail behind only that of collagens [6].

SPARC is of particular interest as it has been identified as a marker of poor prognosis and aggressiveness in a large number of human cancers [7], although its role as a tumor initiator and stimulator of cancer progression is not completely understood. In the case of prostate cancer, SPARC has been shown to be predominantly protumorigenic [3,4,8]. Two animal model studies have investigated the role of SPARC in the initiation and progression of prostate cancer, each by breeding SPARC KO mice with TRAMP (transgenic adenocarcinoma of the mouse prostate) mice. Wong et al., building on previous gene expression analyses wherein it was determined that SPARC expression was decreased in highly metastatic prostate cancer cells [9], found that heterozygous or homozygous loss of SPARC expression in TRAMP mice had no effect on the initiation or inhibition of prostate cancer [10]. Thus, this study demonstrates that prostate cancer metastasis is unaltered by partial or a complete absence of SPARC. In contrast, Said et al. [11], using a separate homozygous SPARC KO/TRAMP model, reported SPARC expression to be inhibitory for primary prostate cancer initiation and progression. These findings illustrate the complexity of isolating a function for SPARC in primary prostate carcinogenesis, which may be dependent on the level of SPARC expression or the background of the mice tested. One additional limitation of the TRAMP prostate carcinogenesis model is a lack of bone metastases precluding the use of this model for isolating a role of SPARC in prostate cancer bone metastasis.

We have previously demonstrated that prostate cancer cells migrate toward bone extracts containing SPARC [12]. Exogenous SPARC was also shown to act as a chemotactic factor by inducing prostate cancer migration [8,13]. Thus, SPARC seems to be a promoter of a promigratory and invasive phenotype of prostate cancer cells *in vitro*. Conversely, several studies have reported the hypermethylation of SPARC in prostate cancer tissues and in prostate cancer cells [9,14]. Therefore, a loss of endogenous SPARC expression by cancerous cells results in their progression, and the levels of SPARC in the tumor and stroma may differentially affect prostate cancer progression. Interestingly, coculture of bone marrow and prostate cancer cells resulted in increased SPARC expression and secretion [15]. Further, in an *in vivo* model of prostate cancer growth in human bones implanted in mice, SPARC expression was found in tumor cells, the bone matrix, and stromal cells [15]. In addition, we have previously demonstrated that SPARC expression is increased in bone metastasis compared with the primary tumor [12]. Thus, SPARC expression may have different functions at primary and secondary tumor sites.

Nevertheless, it is unclear whether SPARC affects the development of tumor-induced bone lesions and whether stromal SPARC affects the expansion of bone lesions. In this study, we investigate the consequences of SPARC deficiency within the tumor environment, but not the tumor itself, on prostate cancer growth within the bone and on bone lesion progression. For this purpose, we used SPARC-deficient mice that received direct intraosseous injections of SPARC-expressing syngeneic RM1 mouse prostate cancer cells. As such, we have used a model wherein stromal SPARC expression is absent, while tumor expression of SPARC remains. Our data illustrate an inhibitory role for bone stromal SPARC in prostate cancer expansion in bone through the regulation of osteoclast formation and function.

Materials and Methods

Mice and Cells

SPARC KO and SPARC WT mice of the same genetic background (B6;129S) were a kind gift from Dr E.H. Sage and were backcrossed to a C57BL/6 background for more than eight generations [16]. RM1 murine prostate cancer cells were provided by Dr W. Heston (Cleveland Clinic) and routinely cultured in RPMI 1640 supplemented with 10% heat-inactivated FBS, 100 U/ml penicillin, and 100 μg/ml streptomycin with passage by trypsinization (0.05% trypsin, 0.53 mM EDTA). Cells were used up to passage 12.

Intraosseous Implantations

Male 10- to 12-week-old SPARC KO or SPARC WT littermates were anesthetized by intraperitoneal injection of 100 mg/kg ketamine and 10 mg/kg xylazine. Intratibial injections have been described previously [17]. In brief, the knee area was prepared by shaving then scrubbing with a chlorhexidine solution. The knee was flexed, and a hole was formed in the proximal end of the tibia using a 27-gauge needle. A 29-gauge insulin needle/syringe was then inserted into this cortical opening to deliver RM1 cells (1×10^3 cells) in suspension (PBS) to the marrow space of the tibial metaphysis just distal to the growth plate. The contralateral tibia was injected with PBS alone as a control (sham injection). All animal procedures were performed in accordance with an approved institutional protocol according to the guidelines of the Institutional Animal Care and Use Committee of the Cleveland Clinic.

Micro–Computed Tomography Analysis

Micro–computed tomography (microCT) analysis of tibiae was performed 1 day after cell implantation and after 14 days of tumor growth. Scans were conducted in the Cleveland Clinic Biomedical Imaging and Analysis Core Center on a GE eXplore Locus microCT (GE Healthcare, Piscataway, NJ) and 360 X-ray projections were collected in 1° increments (80 kV [peak], 500 mA, 26 minutes of total scan time). Projection images were preprocessed and reconstructed into three-dimensional volumes (1024^3 voxels, 20-μm resolution) on a 4PC reconstruction cluster using a modified tent-FDK cone-beam algorithm (GE reconstruction software). Three-dimensional data were processed and rendered (isosurface/maximum-intensity projections) using MicroView (GE Healthcare). For each volume, a plane perpendicular to the *z*-axis/tibial shaft was generated and placed at the base of the growth plate. A second, parallel plane was defined 1.0 mm below, and the entire volume was cropped to this volume of interest for quantitative analysis. Image stacks from each volume of interest were exported for quantitative analysis. Cancellous bone masks were generated in MicroView, and three-dimensional trabecular structural indices were extracted using custom MatLab (The MathWorks, Inc, Natick, MA) algorithms. Trabecular thickness (Tb.Th) and trabecular spacing (Tb.Sp) were determined by previously reported methods [18]. Trabecular number (Tb.N) was calculated by taking the inverse of the average distance between the medial axes of trabecular bone

segments. Bone volume fraction (BV/TV, total bone voxels divided by total cancellous bone mask voxels) and bone surface area (BSA, sum of pixels along edges of trabecular bone) were also calculated for each VOI.

Bone Histology

Fourteen days after cancer cell implantation, mice were sacrificed. Bilateral tibiae, both tumor-bearing and contralateral control, were removed and decalcified in EDTA during a 2-week period. Tibiae were then processed for embedding in paraffin, and sections were cut for staining with hematoxylin and eosin (H&E) to visualize tumors and associated bone destruction. Separately, osteoclasts were stained for tartrate-resistant acid phosphatase (TRAP) expression (0.1 mg/ml naphthol AS-MX phosphate disodium salt, 0.01% [vol./vol.] Triton X-100, 0.03 M sodium tartrate, 0.015 M acetic acid, 0.035 M sodium acetate, and 0.3 mg/ml Fast Red Violet LB). Slides were counterstained with Gill's No. 3 hematoxylin solution. All chemicals were from Sigma-Aldrich (St Louis, MO). Images were taken with a Leica DM2500 light microscope (Leica Microsystems, Bannockburn, IL).

Osteoclast Formation and Function

Tibiae and femurs were isolated from SPARC KO and SPARC WT mice, and the bone ends were removed. Bone marrow (BM) was flushed with PBS containing penicillin and streptomycin. Cell clumps were dispersed by passing consecutively through 18-gauge and 21-gauge needles. Isolated cells were plated (1×10^6) in α modified Eagle medium (αMEM) containing 10% FBS, penicillin and streptomycin, and 100 ng/ml murine macrophage colony-stimulating factor (M-CSF; R&D Systems, Minneapolis, MN). After 3 days, adherent BM-derived macrophages (BMMΦ) were stained with F4/80 Ab (AbD Serotec, Raleigh, NC) followed by Alexa 488 (Life Technologies Corp, Carlsbad, CA). 4′,6-Diamidino-2-phenylindole (DAPI) was used as a nuclear stain. Cell counts and F4/80 positivity were determined using Image Pro software (Media Cybernetics, Inc, Bethesda, MD). Separately, adherent BMMΦs, grown in αMEM containing M-CSF (100 ng/ml) for 3 days, were washed in cold PBS, and placed on ice for 30 minutes. Cells were lifted and plated (5×10^5) in αMEM containing M-CSF (30 ng/ml) with receptor activator of NF-κB ligand (RANKL; 100 ng/ml) on BD BioCoat Osteologic Multitest slides (BD Biosciences, Bedford, MA) or Lab-Tek Chamber slides (Nunc, Rochester, NY). Medium was replaced 2 days after plating, and slides were examined 5 days after plating. Cells on Osteologic slides were removed by incubating with bleach, washed, and allowed to air dry. Cells in chamber slides were fixed in 10% glutaraldehyde for 15 minutes at 37°C then stained for TRAP expression. Ten images per well were taken with a light microscope (DM2500; Leica Microsystems). Image Pro software (Media Cybernetics) was used to calculate total pit area and average pit area on Osteologic slides. Alternatively, the total number of TRAP-positive and cells containing more than 3 nuclei (MNC; multinuclear cells) was counted.

Osteoclast Coculture

BM was isolated from the bones of SPARC WT and KO mice and cultured in αMEM containing 100 ng/ml M-CSF for 3 days. The resulting BMMΦs were either plated alone (1.8×10^4 cells/cm^2) or in coculture with RM1 cells (1:10; 1.6×10^4 cells/cm^2 BMMΦs, 0.2×10^4 cells/cm^2 RM1). In addition, RM1 cells were plated alone (0.2×10^4 cells/cm^2). Cultures were maintained in αMEM containing 100 ng/ml M-CSF in chamber slides and stained for TRAP expression after 5 days.

Osteoclast Resorption of Parietal Bones

Parietal bones from SPARC KO and SPARC WT mice were harvested and then devitalized by placing bones in 70% ethanol and freezing at −80°C. Bones were cut into a circle with a hole punch and placed

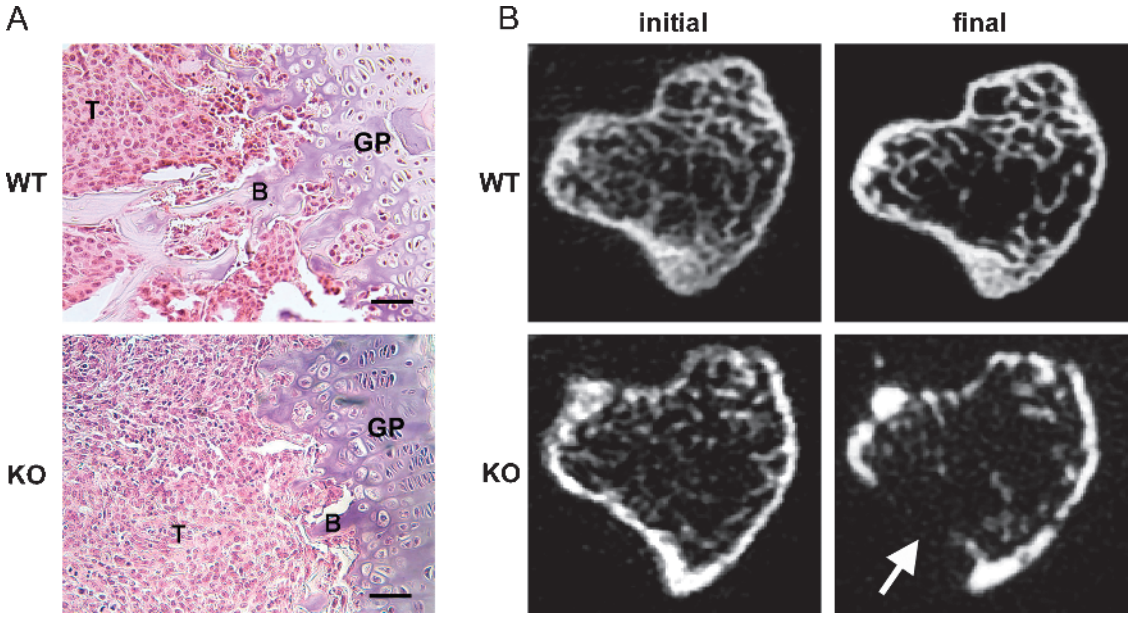

Figure 1. SPARC deficiency stimulates osteolysis. RM1 cells (1×10^3) were injected into the tibia of SPARC WT or KO mice. (A) Bones were isolated after 2 weeks of intraosseous growth, sectioned, and stained with H&E. RM1 cells (T) can be seen growing in the proximal metaphysis and have completely replaced the bone marrow. B indicates trabecular bone; GP, growth plate. Scale bars, 50 μm. (B) MicroCT-derived transaxial slices from mice 1 day (initial) and 2 weeks (final) after tumor implantation. Severe osteolysis can be seen in KO mice. Arrow indicates site of cortical breach. Representative images from nine mice are shown.

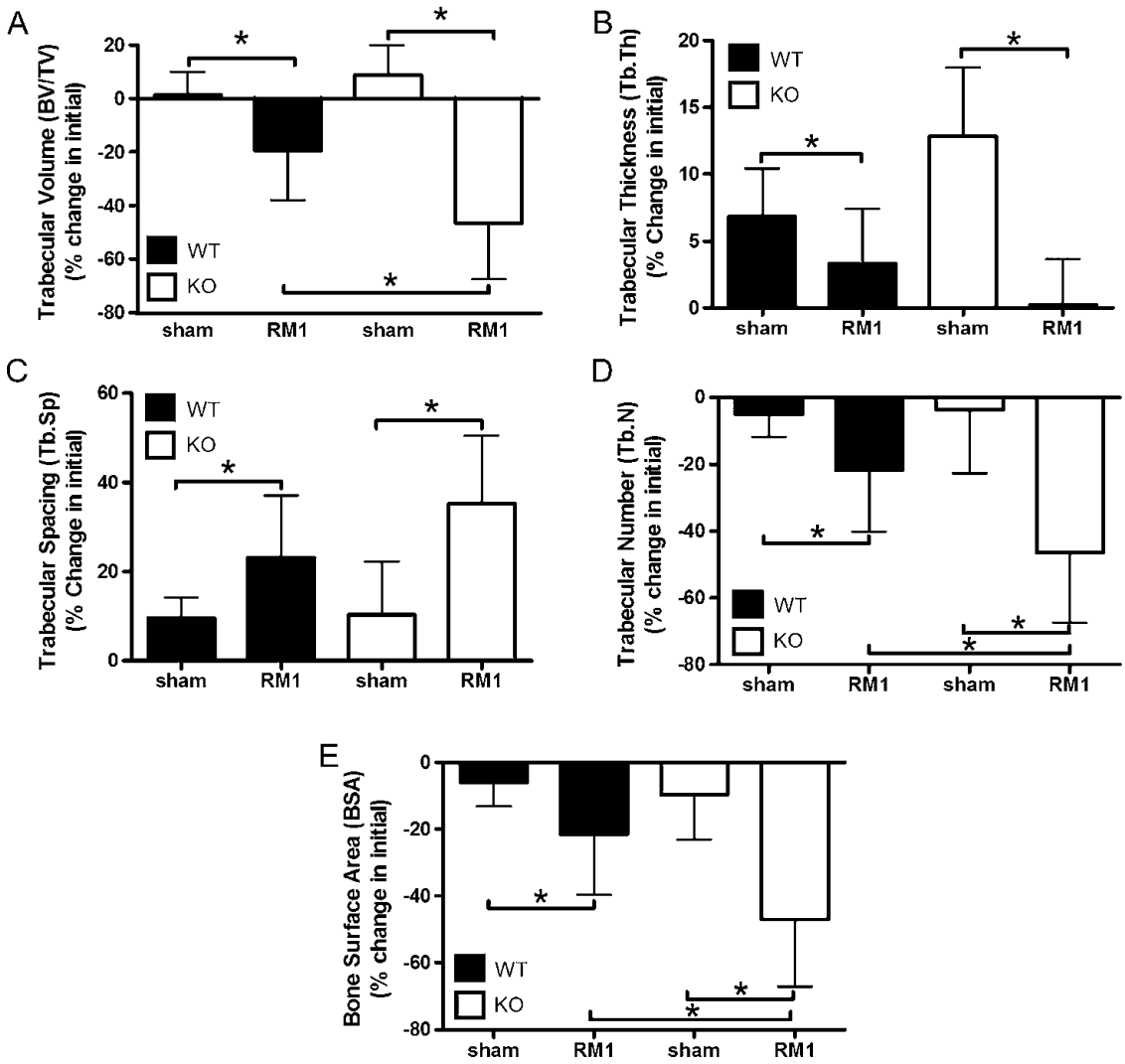

Figure 2. SPARC deficiency triggers enhanced bone resorption. RM1 (1×10^3) cells were injected into the tibia of SPARC WT (black columns) or KO (white columns) mice. Sham PBS injections were performed on the contralateral leg. MicroCT was used to determine bone morphometric changes in (A) BV/TV, (B) Tb.Th, (C) Tb.Sp, (D) Tb.N, and (E) BSA. Values were represented as mean percentage change from initial ± SD measured for nine mice per group. $^*P < .05$ by one-way ANOVA.

in the wells of a 96-well plate containing PBS. After 1 hour in a cell culture incubator at 37°C with 5% CO_2, PBS was removed and BMMΦ was isolated from SPARC KO or SPARC WT mice in αMEM containing M-CSF (30 ng/ml) and RANKL (100 ng/ml) were added to the wells. After 5 days, with medium replaced on day 3, bones were removed and placed in bleach followed by a rinse in water. Bones were visualized and photographed using a Leica DM2500 light microscope at 10 different visual planes. The 10 images were compiled into a single "optimal" image using Image Pro software. Pit areas were quantified using National Institutes of Health ImageJ.

Statistical Analysis

Analysis of variance (one-way) followed by Tukey multiple comparison test or Student's *t* test were used to calculate statistical significance (GraphPad Prism 5.0, La Jolla, CA). Differences were considered significant when $P < .05$. All data depicted and described in text are mean ± SD. $^*P < .05$, $^{**}P < .01$, and $^{***}P < .005$.

Results

Stromal SPARC Suppresses Prostate Cancer–Induced Osteolysis

Bones of SPARC KO mice were previously shown to contain reduced trabecular morphometric parameters and associated diminished bone quality and strength as a result of reduced numbers of osteoblast precursors and reduced osteoblast function owing to progressive low-turnover osteopenia [19]. Our own morphometric values determined by microCT confirmed reduced trabecular numbers and morphometric parameters (Figure W1). Using SPARC- and RANKL-expressing RM1 murine prostate cancer cells (Figure W2) injected directly into the tibial metaphysis of SPARC KO mice, we investigated the role of bone stromal SPARC on the progression of bone-residing prostate cancer and on bone lesion expansion. SPARC WT bones after RM1 injection exhibited robust SPARC expression in the stromal cells, including bone marrow and vasculature, with moderate expression by the RM1 cells and growth plate chondrocytes, whereas SPARC KO bones only

displayed SPARC staining in the tumor with negligible stromal expression (Figure W3).

We recently characterized a model of intratibial RM1 injection as a method to investigate prostate cancer: stromal interactions within the bone of immune-competent syngeneic mice [17] and reported that RM1 cells rapidly expand within bone secondary to a robust osteolytic response. As expected, prostate cancer expansion proceeded rapidly in the tibiae of both SPARC WT and KO mice resulting in the displacement of bone marrow in the metaphysis (Figure 1*A*). Prostate cancer growth in SPARC KO mice resulted in a loss of trabecular bone beneath the growth plate (Figure 1*A*). Whereas microCT-derived individual transaxial slices within the secondary spongiosa of SPARC WT and KO mice illustrated rapid osteolysis in both SPARC WT and KO animals (Figure 1*B*), the lytic response in KO mice was more robust and included a cortical breach (Figure 1*B*, *arrow*). Quantification of morphometric changes in a region distal to the metaphyseal growth plate of injected tibiae indicated an approximately two-fold greater reduction in trabecular bone volume (BV/TV) in SPARC KO mice compared with WT mice (Figure 2*A*). Corresponding trends were noted for Tb.Th and Tb.Sp, although the differences between SPARC WT and KO were not significant (Figure 2, *B* and *C*). The Tb.N in SPARC KO mice was significantly lower than WT (Figure 2*D*), corresponding with our histologic data (Figure 1*A*). In concert with the changes in BV/TV and Tb.N, the total BSA was lower in SPARC KO mice compared with WT (Figure 2*E*). Thus, a loss of stromal SPARC results in enhanced osteolysis on prostate cancer implantation. No significant changes in the bone structure indices were seen between sham-operated SPARC WT and KO mice (Figure 2). Moderately osteolytic B16-F10 murine melanoma cells, when implanted into the tibia of SPARC WT and KO mice, expanded but failed to promote extensive osteolysis (Figure W4). Thus, this enhanced osteolysis in SPARC KO mice is the result of bone-residing prostate cancer and not merely an effect of tumor presence.

Osteoclast Numbers Are Increased in the Presence of RM1 Cells

Intratibial injection of RM1 cells stimulated osteolysis in SPARC WT and KO mice. We used TRAP staining to visualize osteoclasts in the presence and absence of RM1 cells and to assess their possible contribution to the increased osteolysis (Figure 3, *A*–*H*). The number of TRAP-positive osteoclasts was equal or lower in SPARC KO bone compared with WT after sham injection (Figure 3, *A*, *B*, and *I*), confirming other reports [19]. RM1 growth stimulated increased TRAP staining in both SPARC WT and KO mice in the metaphysis below the epiphyseal growth plate (1.74- and 2.37-fold over sham, respectively; Figure 3, *C*, *D*, and *I*). This effect was not seen in mice injected with B16-F10 melanoma cells (Figure W5). Interestingly, numbers of osteoclasts in SPARC KO mice were 1.36-fold higher than in WT mice in the presence of RM1 cells (Figure 3, *C*, *D*, and *I*). In SPARC KO mice injected with RM1 cells, a cortical breach occurred in an area of high osteoclast numbers (Figure 3*D*, *arrow*). Osteoclast numbers were also seen to be increased within a highly remodeling area of cortical bone in the diaphysis (Figure 3, *E* and *F*). Osteoclast numbers in SPARC KO mice are particularly increased along the edges of the RM1 tumor and in the secondary ossification center where remodeling continues to occur after

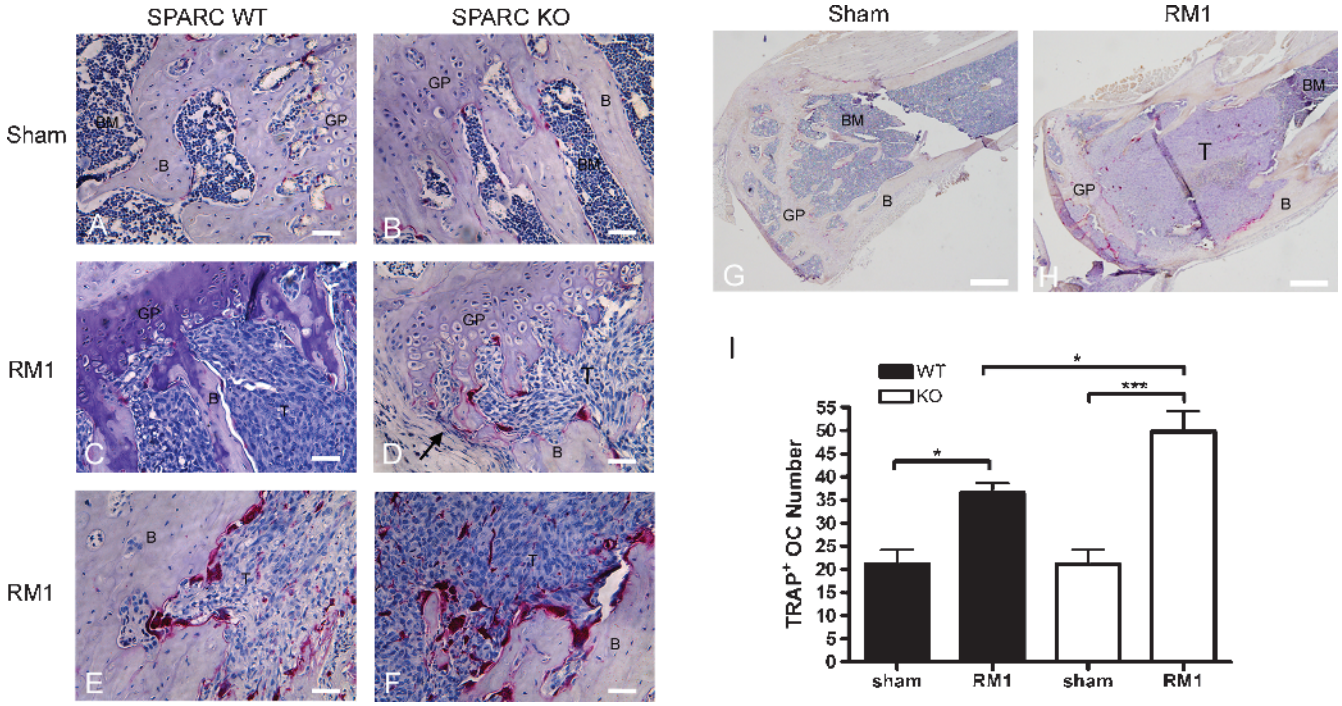

Figure 3. TRAP staining is increased in SPARC KO mice. A sham injection was performed as a control in SPARC WT (A) or KO (B and G) mice. RM1 cells (1×10^3) were injected into the tibia of SPARC WT (C and E) or KO (D, F, and H) mice. Bones were isolated after 2 weeks of intraosseous tumor growth and sectioned. Osteoclasts were visualized by TRAP staining (dark red) and counterstained with hematoxylin. RM1 cells (T) can be seen growing in the proximal metaphysis and have completely replaced the bone marrow (BM). B indicates trabecular bone; GP, growth plate. Arrow indicates site of cortical breach (D). Scale bars, 50 μm (A–D); 200 μm (G and H). Representative images from nine mice are shown. (I) The number of TRAP-stained osteoclasts near the metaphysis of SPARC WT (black columns) or KO (white columns) was counted and represented as mean osteoclast number ± SD ($n = 7$ bones from individual mice). *$P < .05$ and ***$P < .001$ by one-way ANOVA.

loss of the trabeculae (Figure 3*H*) compared with sham injection (Figure 3*G*). Thus, bone-residing RM1 cells stimulate osteoclasts in SPARC WT and KO mice.

RM1 Cell Growth Directly Stimulates Osteoclast Differentiation

To determine whether RM1 growth directly affected osteoclast differentiation, we cocultured RM1 cells with osteoclast progenitors (BMMΦs) generated from SPARC WT and KO bone marrow by treatment with M-CSF. Osteoclastic differentiation of BMMΦs was assessed by TRAP staining and formation of TRAP-positive "osteoclast like" multinucleated cells (MNCs; >3 nuclei; Figure 4*A*). Coculture of BMMΦs with RM1 cells resulted in the formation of 4.2-fold higher in SPARC WT and 7.8-fold higher in SPARC KO cultures compared with BMMΦs cultured alone (Figure 4*B*). Interestingly, the numbers of osteoclasts in SPARC KO cultures were 1.86-fold higher than WT cultures in the presence of RM1 cells (Figure 4*B*). RM1 cells alone demonstrated no TRAP staining, and BMMΦs alone formed less than one MNC per field on average in the presence of M-CSF alone. Thus, RM1 cell growth triggers increased osteoclast formation in both SPARC WT and KO BMMΦ cultures, likely through the production of RANKL. However, osteoclast progenitors in SPARC KO mice may have enhanced differentiation or functional capabilities contributing to the increased osteolysis after tumor challenge.

SPARC Inhibits Osteoclast Maturation and Bone Resorption

Our data derived from microCT and histologic analysis of prostate cancer–induced bone lysis *in vivo* suggest that SPARC KO mice may have an enhanced resorptive capacity on tumor challenge. To determine whether osteoclast progenitor numbers are altered in SPARC KO mice, bone marrow from SPARC WT and KO mice were cultured for 3 days in the presence of M-CSF, and numbers of cells expressing the macrophage marker F4/80 were quantified. Treatment of SPARC KO marrow cultures with M-CSF resulted in a significant increase (1.48-fold) compared with WT cultures, in the number of F4/80–expressing osteoclast progenitor BMMΦ cells (Figure 5*A*), whereas the percentage of cells expressing F4/80 was similar (WT = 89.09% ± 4.38%, KO = 84.37% ± 8.15%). We next examined the osteoclastic differentiation of bone marrow cells from SPARC WT and KO mice by TRAP staining and formation of MNCs (Figure 5*B*). Treatment with M-CSF followed by RANKL resulted in elevated numbers of TRAP-positive "osteoclast-like" MNCs (>3 nuclei) per high-power field in marrow cultures of SPARC KO mice (WT = 5.25 ± 1.42, KO = 6.75 ± 1.91). We next examined osteoclast resorptive capacity using calcium phosphate–coated slides. SPARC KO BMMΦ cells plated on calcium phosphate–coated slides in the presence of M-CSF and RANKL displayed resorptive "pits" of a greater total pit area and mean pit diameter (1.40- and 1.38-fold greater, respectively) compared with WT (Figure 5*C*). These data indicate that osteoclast progenitor sensitivity to M-CSF, a stimulator of proliferation, is enhanced in marrow cultures of SPARC KO mice compared with WT mice leading to a significant increase in the number of F4/80–expressing cells and the formation of multinucleated osteoclast-like TRAP-expressing cells possessing augmented resorptive capacity.

Enhanced Osteolysis Is Due to SPARC-null Osteoclasts, Not Bone Structure

To determine whether the enhanced osteolysis in SPARC KO animals was due to increased osteoclast function or due to altered bone structure, we plated SPARC KO and WT BMMΦs on parietal bones

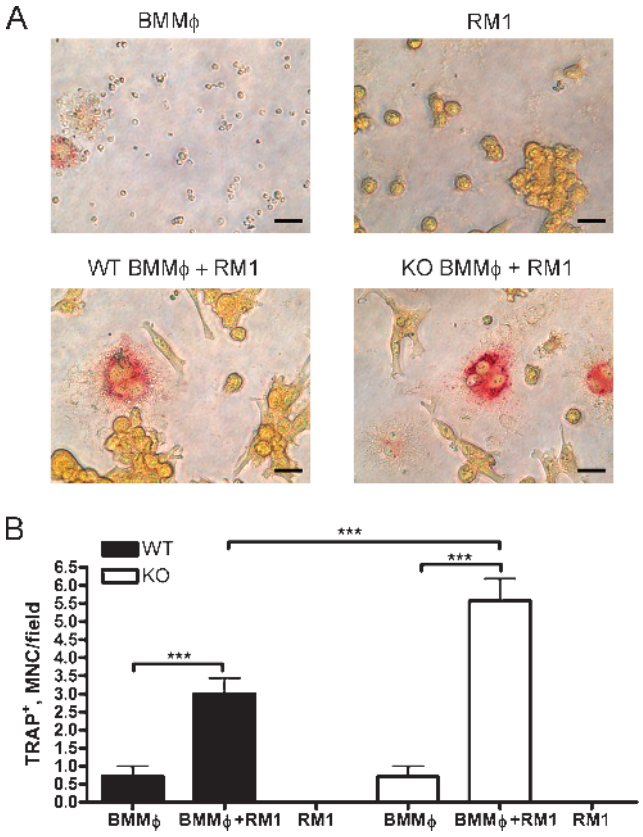

Figure 4. Prostate cancer growth induces osteoclast differentiation. Osteoclast precursors (BMMΦ) were isolated from the bone marrow of SPARC WT (black columns) or KO (white columns) mice. Marrow was flushed and plated in the presence of 100 ng/ml M-CSF. Resulting BMMΦs and RM1 cells were plated alone or in coculture then treated with 100 ng/ml M-CSF for 5 more days and stained for TRAP. (A) Scale bars, 25 μm. (B) TRAP-positive BMMΦs and RM1 cells alone or in coculture were counted and displayed as mean ± SD (n = 7 fields from duplicate experiments). ***P < .001 by one-way ANOVA.

from SPARC KO and WT mice. All cultures displayed large pits (Figure 6*A*). SPARC KO cells resorbed 2.37-fold more bone on SPARC KO and 2.74-fold more on WT bones compared with WT cells (Figure 6*B*). The percent area resorbed by SPARC WT cells was similar on WT and KO bone (WT = 6.07% ± 1.48%, KO = 7.30% ± 1.67%). The altered bone structure due to the SPARC KO did result in 1.39-fold higher resorption by SPARC KO cells compared with the same cells on WT bone (Figure 6*B*). However, the deficiency of SPARC in osteoclasts exerts a greater effect on osteolysis than the altered bone architecture.

Discussion

We recently described a model to investigate prostate cancer: bone stroma interactions in immune competent mice using the murine RM1 prostate cancer cell line and direct intraosseous implantations [17]. Herein, we use this model to elucidate the role of bone stromal SPARC in metastatic prostate cancer progression and bone lesion expansion. Although there are several reports addressing the function of SPARC in prostate cancer initiation and progression [4,10,11], it is unclear whether SPARC present in the bone tissue is involved in tumor-induced lesion progression. The main conclusions from this study are

the following: 1) quantitative microCT analysis of prostate cancer harboring SPARC KO bone reveals an enhanced tumor-induced osteolytic response, 2) prostate cancer growth in the bone marrow cavity stimulates osteoclast formation, which is increased in SPARC KO bones, 3) SPARC KO marrow cultures exhibit increased expansion and augmented formation of TRAP-positive MNC with heightened resorptive capacity, and 4) enhanced osteolysis is due to increased resorption by SPARC KO cells and not solely the altered bone structure. Together, these results suggest that the presence of SPARC in host bone tissues, and associated osteoclasts, limits the osteolysis and bone lesion progression stimulated by prostate cancer cells.

We have previously shown that RM1 cells induce an osteoclast-mediated response in long bones of syngeneic mice leading to elevated serum TRAP [17]. In addition, RM1 cells have the ability to enhance proliferation of RAW264.7 monocyte-macrophage lineage cells [17] and stimulate differentiation of osteoclast progenitors *in vitro*. The model used previously [17] and in this study uses direct implantation of RM1 cells within the marrow space of long bones. We demonstrate that bone-residing RM1 cells stimulate osteoclast formation *in vivo*. Similar to the data presented in our study, osteoclast numbers are increased in patients with prostate cancer bone metastases [20]. In addition, it is apparent that the presence of an expanding bone-residing tumor alone is not sufficient to enhance osteolysis as bone-residing B16-F10 murine melanoma cells did not result in an accentuated osteoclast response. This is supported by the fact that 80% of advanced prostate cancers metastasize to bone compared with only 25% to

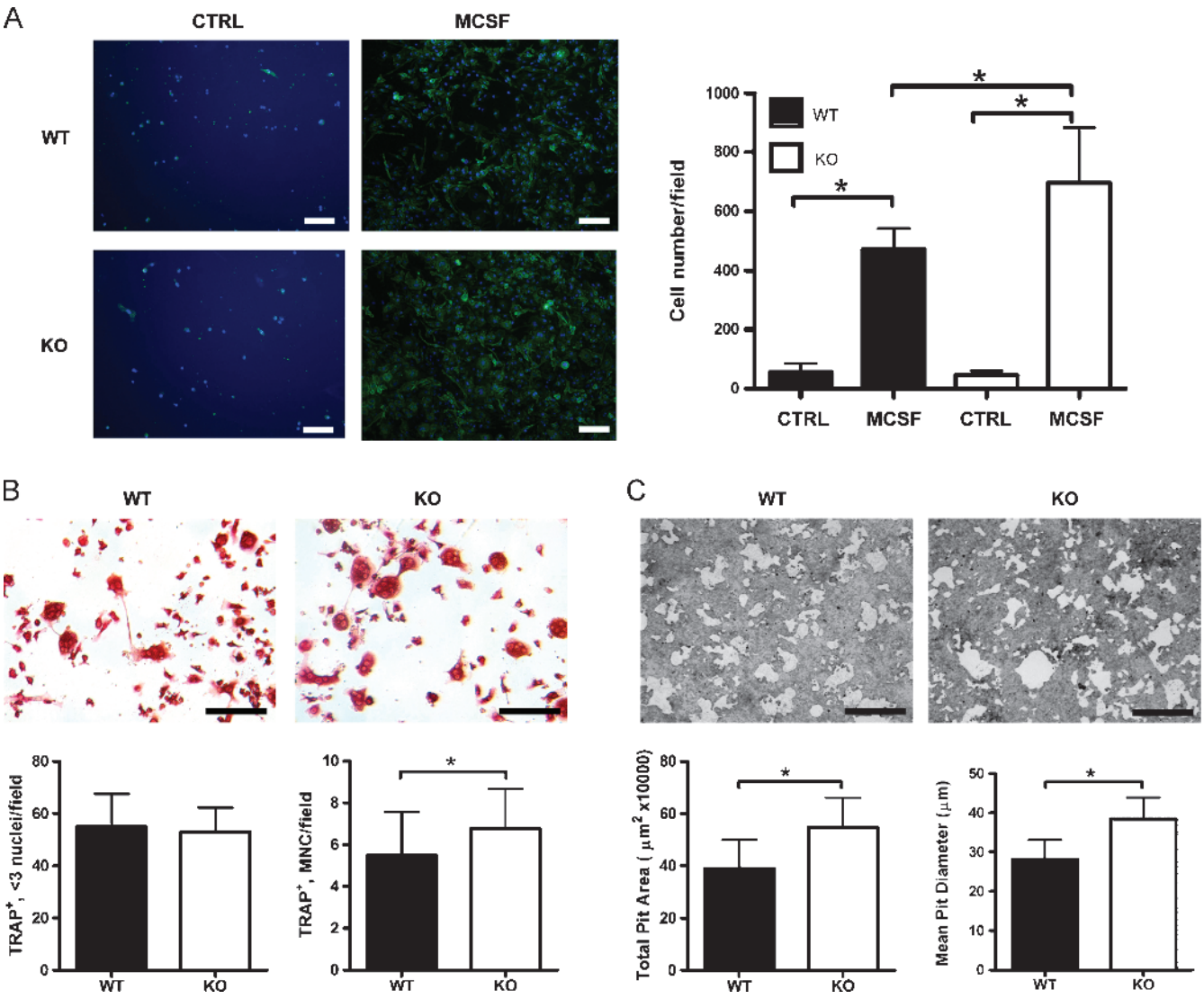

Figure 5. Osteoclast maturation is accelerated in SPARC KO mice. BMMΦs were isolated from the bone marrow of SPARC WT (black columns) or KO (white columns) mice. (A) Marrow was flushed and plated in the presence of 100 ng/ml M-CSF. On the third day, cells were fixed and stained for the macrophage marker F4/80 (green) to visualize BMMΦs. DAPI staining (blue) was used to show total cell numbers. Scale bars, 50 μm. F4/80–positive cells were counted and displayed as mean ± SD (n = 7 fields from triplicate experiments). *P < .05 by one-way ANOVA. (B) BMMΦ cells developed *in vitro* were then treated with 30 ng/ml M-CSF and 100 ng/ml RANKL for 3 more days. Scale bars, 50 μm. Cells were stained for TRAP, counted, and displayed as mean ± SD (n = 12 fields from triplicate experiments). *P < .05 by Student's t test. (C) BMMΦ cells developed *in vitro* were plated, in the presence of 30 ng/ml M-CSF and 100 ng/ml RANKL, on calcium phosphate–coated coverslips. Scale bars, 50 μm. Pit formation was quantified 3 days later with total pit area/field and mean pit diameter was shown as mean ± SD (n = 20 fields from quadruplicate experiments). *P < .05 by Student's t test.

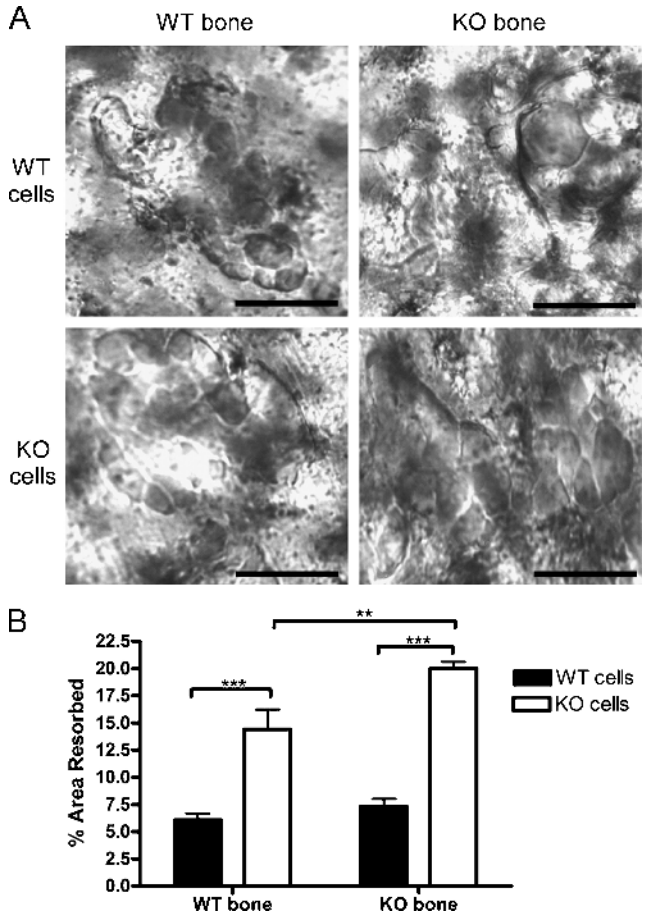

Figure 6. SPARC KO osteoclasts are hyperresorptive. BMMΦs were isolated from the bone marrow of SPARC WT (WT cells, black columns) or KO (KO cells, white columns) mice. Marrow was flushed and plated in the presence of 100 ng/ml M-CSF. After 3 days, 5×10^5 BMMΦ cells were then placed on parietal bones from either SPARC WT (WT bone) or KO (KO bone) mice and treated with 30 ng/ml M-CSF and 100 ng/ml RANKL for 5 more days. (A) Pits formed by osteoclasts were visualized microscopically. Scale bars, 50 μm. Representative images from 10 fields are shown. (B) Pit area was measured and represented as mean percentage area resorbed ± SD (n = 10 fields from duplicate experiments). $^{**}P < .01$ and $^{***}P < .001$ by one-way ANOVA.

49% of advanced melanomas [21,22]. Thus, the RM1 prostate cancer model is more proficient in producing an osteolytic response on implantation into bone.

The RM1 model of prostate cancer bone metastasis has recently been expanded on by Power et al. [23], wherein RM1 cells were conditioned to home to bone after intracardiac injection. In addition, intrafemoral injection of RM1 cells has been used to study bone metastasis and its effects on bone marrow precursors [24]. These two studies open the possibility for the investigation of bone stromal SPARC as a mediator of prostate cancer homing to bone in immune competent mice. Previous studies have illustrated the potential of SPARC as a mediator of prostate cancer migration to bone extracts *in vitro* [8,12,13] or the effects of tumor-expressed SPARC as a mediator of bone homing potential [25], but no studies have investigated bone-resident SPARC as a mediator of osteotropism *in vivo*. In light of studies indicating that active bone remodeling promotes cancer homing to bone [26] and that SPARC KO mice have impaired bone turnover [19], the use of SPARC KO mice to investigate osteotropism of cancers may prove fruitless as gradients of pro–bone-homing factors released from bone during remodeling may be reduced or absent.

Bone remodeling is partially driven by osteoclasts, which are bone-resorbing MNCs formed by the fusion of circulating or hematopoietic tissue, such as bone, residing mononuclear precursors [27]. Differentiation of osteoclasts is governed primarily by M-CSF, RANKL, and levels of osteoprotegrin, a RANKL decoy receptor [28]. We have found that marrow cells from SPARC KO mice have enhanced sensitivity to M-CSF. In light of the larger mean pit size formed by SPARC KO osteoclast-like cells compared with WT, it seems that SPARC restricts osteoclast activity. Our findings that marrow cultures from SPARC KO mice treated with M-CSF and RANKL lead to increased TRAP-positive osteoclast-like cell formation is similar to those reported by Machado do Reis et al. [29]. Despite this increase in osteoclast precursors in SPARC KO mice, there are fewer TRAP staining osteoclasts in the bone of SPARC KO mice under basal conditions [19]. Our data demonstrate that injection of RM1 cells into SPARC KO mice stimulates increased osteoclast formation. In the sham-injected tibiae, SPARC KO mice contain fewer osteoclasts compared with WT. This may be a secondary effect due to decreased osteoblast numbers in SPARC KO mice [19], resulting in lower RANKL levels and reduced osteoclast differentiation. This decrease in differentiation may result in an accumulation of osteoclast progenitors in SPARC KO animals [29]. On implantation of RM1 cells, which produce both transmembrane and soluble RANKL, osteoclast differentiation is stimulated resulting in increased numbers of osteoclasts and enhanced osteolysis. Prostate cancers also produce cathepsin K, whose expression is increased on metastasis to bone [30]. Cathepsin K was recently shown to cleave SPARC in experimental bone metastases [15]. This cleavage of SPARC could inactivate the protein, creating an environment similar to that of the SPARC KO mouse, resulting in enhanced osteolysis and tumor progression. In addition, we demonstrate that these stimulated SPARC KO osteoclasts are more resorptive; further contributing to the increased osteolysis.

Loss of stromal SPARC expression has been linked to enhanced tumor growth in several cancer types [31–33] including prostate [11]. Each of these studies indicated that loss of SPARC expression resulted in reduced quantities of tumor-associated collagen type I. Because collagen type I is a major component of bone and its maturity [34,35] seems to be altered in SPARC KO bone, it is possible that collagen type I may play a role in the enhanced osteolytic response noted in SPARC KO mice in the presence of bone-residing prostate cancer. Our data demonstrate that whereas SPARC WT and KO osteoclasts formed in culture display increased resorption on SPARC KO bones, SPARC KO osteoclasts have increased resorptive activity on SPARC WT and KO bones. Thus, whereas the altered structure of SPARC KO bone due to collagen type I deposition plays a role in enhanced osteolysis, the deficiency of SPARC in osteoclasts plays a greater role.

Our data illustrate a role for SPARC in the progression of bone metastatic prostate cancer where bone stromal SPARC suppresses tumor expansion by limiting osteoclast maturation and function. Lack of bone stromal SPARC is associated with an apparent accentuated osteoclastic response in bones challenged by prostate cancer and illustrates the importance of SPARC not only in the maintenance of normal bone mass and quality [19] but also in the regulation of bone remodeling owing to pathological conditions such as bone metastatic prostate cancer. Because osteolysis is a key component of prostate cancer progression in bone and defines the course of both osteoblastic and osteolytic

bone lesions, these findings represent an important step in the development of new approaches to treat bone metastases.

References

[1] Coleman RE (1997). Skeletal complications of malignancy. *Cancer* **80**, 1588–1594.

[2] Jemal A, Siegel R, Ward E, Hao Y, Xu J, Murray T, and Thun MJ (2008). Cancer statistics, 2008. *CA Cancer J Clin* **58**, 71–96.

[3] Lapointe J, Li C, Higgins JP, van de Rijn M, Bair E, Montgomery K, Ferrari M, Egevad L, Rayford W, Bergerheim U, et al. (2004). Gene expression profiling identifies clinically relevant subtypes of prostate cancer. *Proc Natl Acad Sci USA* **101**, 811–816.

[4] Thomas R, True LD, Bassuk JA, Lange PH, and Vessella RL (2000). Differential expression of osteonectin/SPARC during human prostate cancer progression. *Clin Cancer Res* **6**, 1140–1149.

[5] Dhanasekaran SM, Barrette TR, Ghosh D, Shah R, Varambally S, Kurachi K, Pienta KJ, Rubin MA, and Chinnaiyan AM (2001). Delineation of prognostic biomarkers in prostate cancer. *Nature* **412**, 822–826.

[6] Brekken RA and Sage EH (2000). SPARC, a matricellular protein: at the crossroads of cell-matrix communication. *Matrix Biol* **19**, 816–827.

[7] Podhajcer OL, Benedetti LG, Girotti MR, Prada F, Salvatierra E, and Llera AS (2008). The role of the matricellular protein SPARC in the dynamic interaction between the tumor and the host. *Cancer Metastasis Rev* **27**, 691–705.

[8] Jacob K, Webber M, Benayahu D, and Kleinman HK (1999). Osteonectin promotes prostate cancer cell migration and invasion: a possible mechanism for metastasis to bone. *Cancer Res* **59**, 4453–4457.

[9] Wang Y, Yu Q, Cho AH, Rondeau G, Welsh J, Adamson E, Mercola D, and McClelland M (2005). Survey of differentially methylated promoters in prostate cancer cell lines. *Neoplasia* **7**, 748–760.

[10] Wong SY, Crowley D, Bronson RT, and Hynes RO (2008). Analyses of the role of endogenous SPARC in mouse models of prostate and breast cancer. *Clin Exp Metastasis* **25**, 109–118.

[11] Said N, Frierson HF Jr, Chernauskas D, Conaway M, Motamed K, and Theodorescu D (2009). The role of SPARC in the TRAMP model of prostate carcinogenesis and progression. *Oncogene* **28**, 3487–3498.

[12] De S, Chen J, Narizhneva NV, Heston W, Brainard J, Sage EH, and Byzova TV (2003). Molecular pathway for cancer metastasis to bone. *J Biol Chem* **278**, 39044–39050.

[13] Chen N, Ye XC, Chu K, Navone NM, Sage EH, Yu-Lee LY, Logothetis CJ, and Lin SH (2007). A secreted isoform of ErbB3 promotes osteonectin expression in bone and enhances the invasiveness of prostate cancer cells. *Cancer Res* **67**, 6544–6548.

[14] Kwabi-Addo B, Wang S, Chung W, Jelinek J, Patierno SR, Wang BD, Andrawis R, Lee NH, Apprey V, Issa JP, et al. (2010). Identification of differentially methylated genes in normal prostate tissues from African American and Caucasian men. *Clin Cancer Res* **16**, 3539–3547.

[15] Podgorski I, Linebaugh BE, Koblinski JE, Rudy DL, Herroon MK, Olive MB, and Sloane BF (2009). Bone marrow–derived cathepsin K cleaves SPARC in bone metastasis. *Am J Pathol* **175**, 1255–1269.

[16] Norose K, Clark JI, Syed NA, Basu A, Heber-Katz E, Sage EH, and Howe CC (1998). SPARC deficiency leads to early-onset cataractogenesis. *Invest Ophthalmol Vis Sci* **39**, 2674–2680.

[17] McCabe NP, Madajka M, Vasanji A, and Byzova TV (2008). Intraosseous injection of RM1 murine prostate cancer cells promotes rapid osteolysis and periosteal bone deposition. *Clin Exp Metastasis* **25**, 581–590.

[18] Hildebrand T, Laib A, Muller R, Dequeker J, and Ruegsegger P (1999). Direct three-dimensional morphometric analysis of human cancellous bone: microstructural data from spine, femur, iliac crest, and calcaneus. *J Bone Miner Res* **14**, 1167–1174.

[19] Delany AM, Amling M, Priemel M, Howe C, Baron R, and Canalis E (2000). Osteopenia and decreased bone formation in osteonectin-deficient mice. *J Clin Invest* **105**, 915–923.

[20] Roato I, D'Amelio P, Gorassini E, Grimaldi A, Bonello L, Fiori C, Delsedime L, Tizzani A, De Libero A, Isaia G, et al. (2008). Osteoclasts are active in bone forming metastases of prostate cancer patients. *PLoS ONE* **3**, e3627.

[21] American Cancer Society (2008). *Melanoma Skin Cancer*. American Cancer Society, Atlanta, GA.

[22] American Cancer Society (2008). *Prostate Cancer*. American Cancer Society, Atlanta, GA.

[23] Power CA, Pwint H, Chan J, Cho J, Yu Y, Walsh W, and Russell PJ (2009). A novel model of bone-metastatic prostate cancer in immunocompetent mice. *Prostate* **69**, 1613–1623.

[24] Tourkova IL, Yamabe K, Chatta G, Shurin GV, and Shurin MR (2003). NK cells mediate Flt3 ligand–induced protection of dendritic cell precursors *in vivo* from the inhibition by prostate carcinoma in the murine bone marrow metastasis model. *J Immunother* **26**, 468–472.

[25] Koblinski JE, Kaplan-Singer BR, VanOsdol SJ, Wu M, Engbring JA, Wang S, Goldsmith CM, Piper JT, Vostal JG, Harms JF, et al. (2005). Endogenous osteonectin/SPARC/BM-40 expression inhibits MDA-MB-231 breast cancer cell metastasis. *Cancer Res* **65**, 7370–7377.

[26] Schneider A, Kalikin LM, Mattos AC, Keller ET, Allen MJ, Pienta KJ, and McCauley LK (2005). Bone turnover mediates preferential localization of prostate cancer in the skeleton. *Endocrinology* **146**, 1727–1736.

[27] Fujikawa Y, Quinn JM, Sabokbar A, McGee JO, and Athanasou NA (1996). The human osteoclast precursor circulates in the monocyte fraction. *Endocrinology* **137**, 4058–4060.

[28] Teitelbaum SL (2000). Bone resorption by osteoclasts. *Science* **289**, 1504–1508.

[29] Machado do Reis L, Kessler CB, Adams DJ, Lorenzo J, Jorgetti V, and Delany AM (2008). Accentuated osteoclastic response to parathyroid hormone undermines bone mass acquisition in osteonectin-null mice. *Bone* **43**, 264–273.

[30] Brubaker KD, Vessella RL, True LD, Thomas R, and Corey E (2003). Cathepsin K mRNA and protein expression in prostate cancer progression. *J Bone Miner Res* **18**, 222–230.

[31] Brekken RA, Puolakkainen P, Graves DC, Workman G, Lubkin SR, and Sage EH (2003). Enhanced growth of tumors in SPARC null mice is associated with changes in the ECM. *J Clin Invest* **111**, 487–495.

[32] Puolakkainen PA, Brekken RA, Muneer S, and Sage EH (2004). Enhanced growth of pancreatic tumors in SPARC-null mice is associated with decreased deposition of extracellular matrix and reduced tumor cell apoptosis. *Mol Cancer Res* **2**, 215–224.

[33] Said N and Motamed K (2005). Absence of host-secreted protein acidic and rich in cysteine (SPARC) augments peritoneal ovarian carcinomatosis. *Am J Pathol* **167**, 1739–1752.

[34] Boskey AL, Moore DJ, Amling M, Canalis E, and Delany AM (2003). Infrared analysis of the mineral and matrix in bones of osteonectin-null mice and their wild type controls. *J Bone Miner Res* **18**, 1005–1011.

[35] Trombetta JM and Bradshaw AD (2010). SPARC/osteonectin functions to maintain homeostasis of the collagenous extracellular matrix in the periodontal ligament. *J Histochem Cytochem* **58**, 871–879.

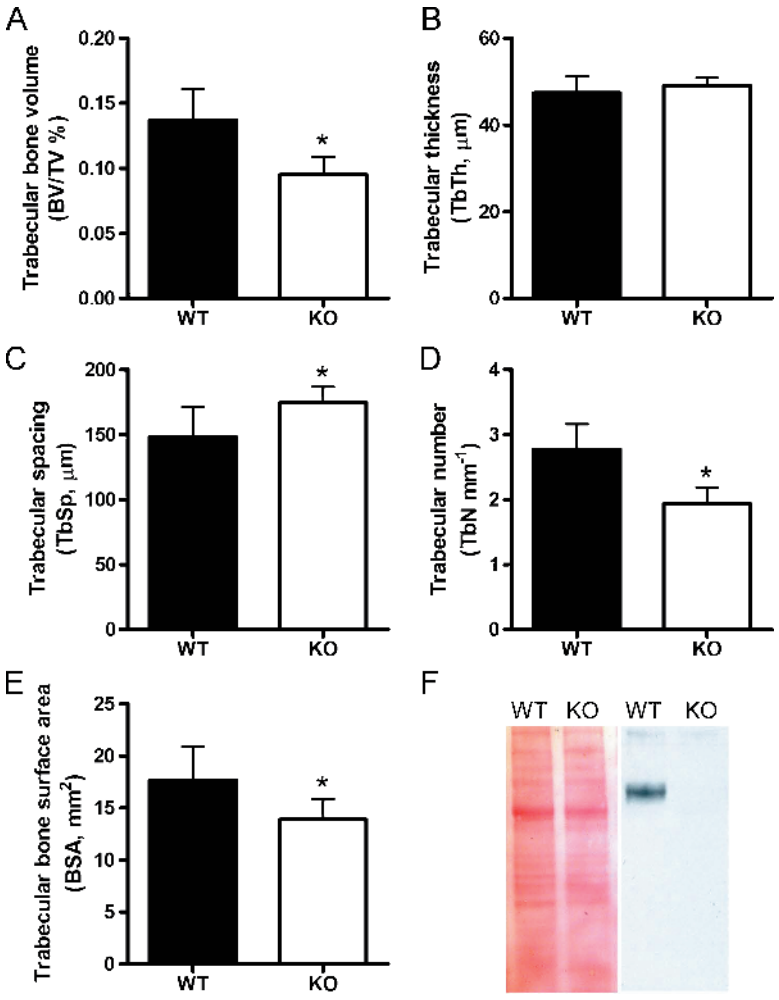

Figure W1. SPARC KO tibia display decreased trabecular morphometric parameters. (A–E) MicroCT was used to determine the bone morphometric parameters of SPARC WT (black columns) and KO (white columns) mice: (A) BV/TV, (B) Tb.Th, (C) Tb.Sp, (D) Tb.N, and (E) BSA. Values were represented as mean ± SD measured for nine mice. *$P < .05$ by Student's t test. (F) Whole bone extracts from femurs of SPARC WT and KO mice lysed with RIPA buffer and separated by SDS-PAGE (4%-12%). (Left) Ponceau S (Sigma)–stained nitrocellulose and (right) immunoblot analysis for SPARC (R&D Systems).

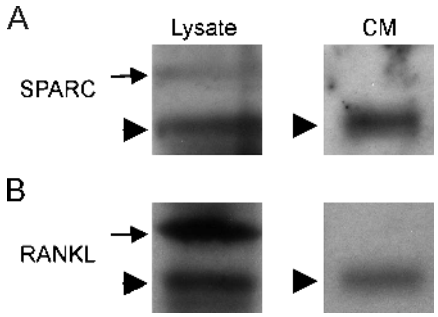

Figure W2. RM1 cells express and secrete SPARC and RANKL. RM1 culture lysates and conditioned medium (CM) were collected. Proteins were separated by SDS-PAGE (10%) followed by (A) SPARC and (B) RANKL (Santa Cruz Biotechnology) immunoblot analysis. Both total (SPARC) or transmembrane (RANKL) (arrow) and soluble (arrowhead) forms of the proteins were found.

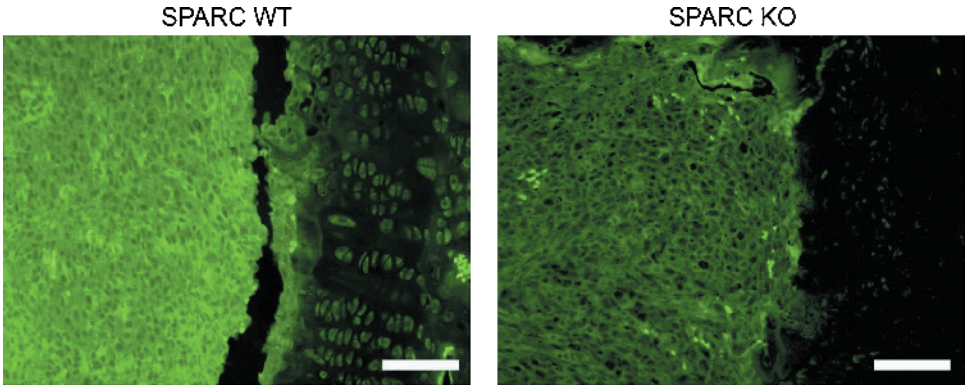

Figure W3. RM1 cells produce SPARC *in vivo*. RM1 cells (1×10^3) were injected into the tibia of SPARC WT or KO. Bones were isolated after 2 weeks of intraosseous tumor growth and paraffin-embedded bone sections were stained for SPARC (green) using a method modified from Trombetta and Bradshaw (*J Histochem Cytochem* 2010;58:871–879). In brief, sections were deparaffinized, rehydrated, and blocked in 2% donkey serum/0.2% Triton X-100/PBS. Slides were incubated for 1 hour with SPARC antibody (R&D Systems) followed by incubation with an antigoat secondary antibody conjugated to Alexa 488 (Molecular Probes). Coverslips were mounted with Vectashield (Vector Laboratories, Burlingame, CA). Images were taken with a Leica DM2500 light microscope. Scale bars, 50 μm. Representative images from nine mice are shown.

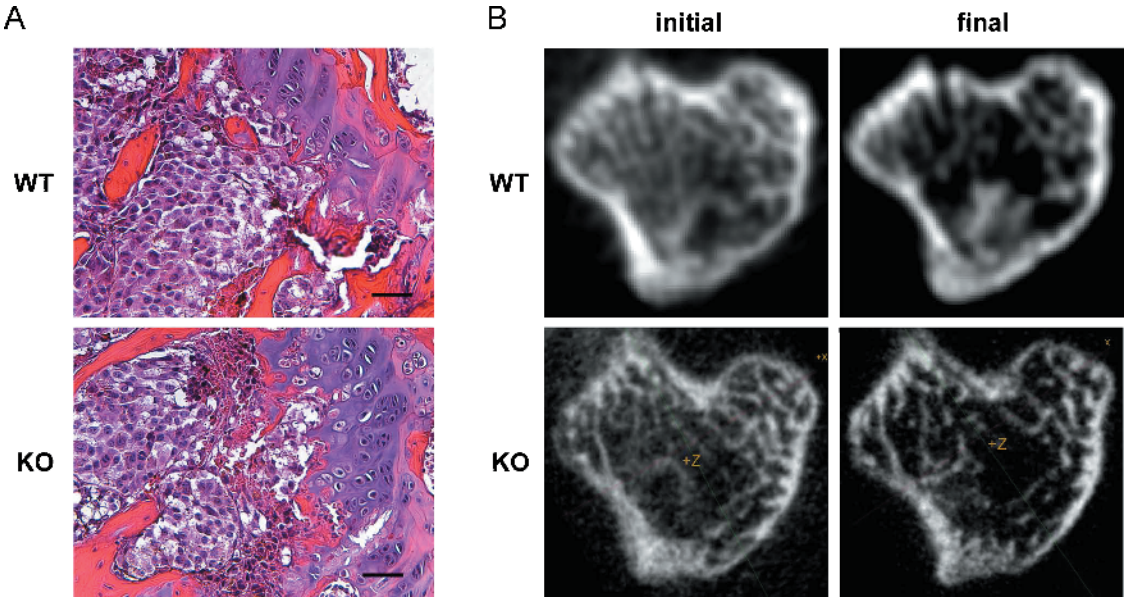

Figure W4. Melanoma implantation does not promote osteolysis. B16-F10 murine melanoma cells (1×10^4) were injected into the tibiae of SPARC WT and KO mice. (A) Bones were isolated after 2 weeks of intraosseous tumor growth, sectioned, and stained with H&E. B16-F10 cells can be seen growing within proximal metaphysis. Scale bars, 50 μm. (B) MicroCT-derived proximal metaphyseal transaxial slices of the tibiae both 1 day (initial) and 2 weeks (final) after B16-F10 cell implantation. Representative images from nine mice are shown.

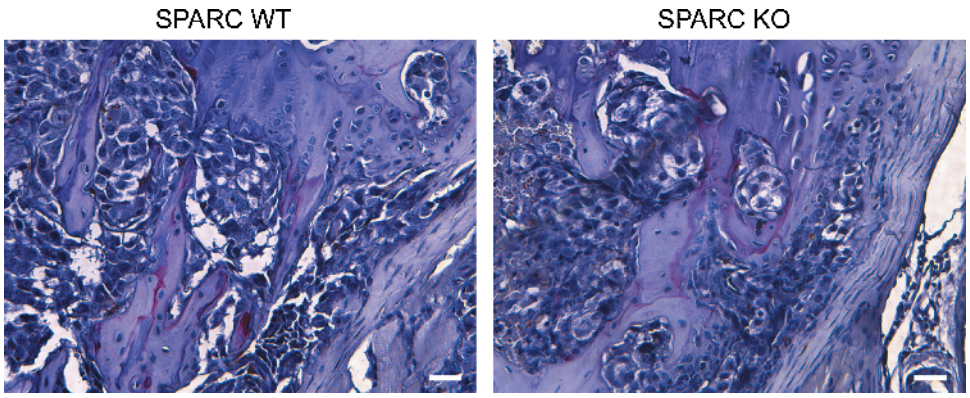

Figure W5. Melanoma implantation does not stimulate osteoclast differentiation. B16-F10 cells (1×10^4) were injected into the tibia of SPARC WT or KO mice. Bones were isolated after 2 weeks of intraosseous tumor growth and sectioned. Osteoclasts were visualized by TRAP staining (dark red) and counterstained with hematoxylin. Scale bars, 50 μm. Representative images from nine mice are shown.